SILVER AND ZINC NANOPARTICLES BIOSYNTHESIS USING LAUREL EXTRACT AND INVESTIGATION OF THE PHOTOCATALYTIC PROPERTIES

Recep Taş [ID][a], Ebru Köroğlu [ID][a], Ahmet Karakuş [a], Ali Savaş Bülbül [b], Nilay Akkuş Taş [c*]

[a]Department of Biotechnology, Faculty of Science, Bartin University,
Kutlubey-Yazıcılar Campus, Bartin 74100, Turkey
[b]Department of Emergency Aid and Disaster Management, Faculty of Applied Sciences, Bayburt University,
Gençosman Neighborhood, 21, February str., Dede Korkut Complex, Bayburt 69000, Turkey
[c]Department of Chemistry, Faculty of Arts and Sciences, Amasya University, Tavşanlı str.,
İpekköy Campus, Amasya 05100 Turkey
[*]e-mail: nilayakkustas@amasya.edu.tr

Abstract. Metal nanoparticles that are widely studied in optoelectronics, catalysis, medicine, and sensors offer remarkable optical and electronic properties. To address the cost and environmental concerns associated with their synthesis, this study employs an environmentally friendly method using *Laureus nobilis* extract to produce silver and zinc nanoparticles, which are prominent in nanotechnology. This study includes investigations of factors such as reaction time, $AgNO_3$/laurel ratio, $Zn(Ac)_2 \cdot H_2O$/laurel ratio and temperature in nanoparticle biosynthesis to optimize the process. The next stage was set to evaluate the photocatalytic performance of these nanoparticles, specifically against the methylene blue dye under dark and UV light conditions. Parameters such as pollutant decomposition, degradation rate, catalyst stability, and nanoparticle recovery were analysed. Structural characterization of the obtained nanoparticles was performed using UV-Vis, FTIR, SEM, and XRD techniques. The photocatalytic results showed significant degradation percentages for LB-AgNP (silver nanoparticles synthesized with *Laureus nobilis* extract) (97.5%) and LB-ZnNP (zinc nanoparticles synthesized with *Laureus nobilis* extract) (90.9%). LB-ZnNP showed superior performance. Therefore, LB-AgNP and LB-ZnNP are promising photocatalysts for water purification and the elimination of toxic organic pollutants.

Keywords: biosynthesis, silver, zinc, nanoparticle, photocatalysis, laurel extract.

Introduction

Nanotechnology is an important and active field of modern science. Biosynthesis in nanotechnology involves the production of nanoparticles using living organisms, such as plants, microorganisms, and fungi, and is often referred to as green chemistry for metallic nanoparticles [1]. Biosynthesis is now a widely used method, but meeting all the criteria of green chemistry, such as safety, one-step reactions, minimal waste, renewable resources, environmental friendliness, easy product separation, and 100% yield, can be challenging in practice [2-5]. The use of metal and metal oxide nanoparticles such as Ag, Cu, TiO_2, and ZnO in antibacterial applications is increasing because of their higher reactivity compared with bulk materials [6]. Ag and ZnO nanoparticles are used as both stabilizing and reducing agents in manufacturing processes. Silver nanoparticles are characterized by high electrical conductivity and local surface plasmon resonance properties [7]. Among metal oxide nanoparticles, ZnO nanoparticles are more significant than other metal oxide nanoparticles because of their catalytic and chemical activities, piezoelectric properties, UV protection capabilities, and availability [8,9]. In addition, ZnO is a white inorganic semiconductor and water-insoluble material found in the structure of certain enzymes, proteins, and hormones [10,11]. Plant material are a good option for use in nanoparticle synthesis because they do not contain toxic chemicals and can directly synthesize natural reducing agents. For example, gold and silver nanoparticles can be obtained from plant extracts [2,3]. The laurel plant (*Laurus nobilis*) grows in the Mediterranean and southeastern Europe. The essential oil of the laurel plant contains several active compounds such as terpineol and cineole. These compounds may have

antimicrobial, antifungal, hypoglycemic, and antiulcerogenic properties [12].

Photocatalysis uses light energy to initiate and accelerate chemical reactions. In recent years, the photocatalytic properties of metal nanoparticles have attracted considerable attention. These properties allow efficient utilization of light through photocatalytic reactions occurring on the surfaces of semiconductor nanoparticles. In particular, silver and zinc nanoparticles have become particularly attractive for photocatalytic applications [13-15].

Silver nanoparticles exhibit strong photocatalytic activity because of their large surface area and plasmonic properties. When stimulated by ultraviolet or visible light, the electrons on the surface of these nanoparticles can be excited, leading to the generation of free radicals and contributing to photocatalytic reactions. These properties have enabled silver nanoparticles to find potential applications in various fields such as antimicrobial activity, water purification, air pollution control, and solar energy conversion [16,17].

In contrast, zinc nanoparticles also have photocatalytic properties. Zinc is a semiconductor metal involved in photocatalytic reactions. The photocatalytic activity of zinc nanoparticles is associated with the absorption of light and the generation of electron/hole pairs. These electron/hole pairs can participate in photocatalytic reactions that lead to the degradation of organic pollutants and the removal of harmful compounds. Therefore, zinc nanoparticles have significant potential for photocatalytic applications in areas such as water purification, air ventilation systems, and solar cells [18-20].

The goal of this study was to investigate the biosynthesis and photocatalytic activity of silver and zinc nanoparticles using laurel extract. The synthesized nanoparticles were characterized using UV-Vis and FTIR spectroscopy, SEM (scanning electron microscopy), and XRD (X-ray diffraction) techniques. The degradation percentages of methylene blue dye, chosen as an organic pollutant, were evaluated after photocatalytic processes in the dark and under UV light using the synthesized nanoparticles.

Experimental
Materials

Reagents including silver nitrate, zinc acetate, and methylene blue and solvents such as ethanol (98%), methanol (99%), acetonitrile (99%), and chloroform (99%) were commercially purchased from Sigma-Aldrich.

Methods

Various devices were used to characterize the synthesized nanoparticles. The UV-3600 Plus Shimadzu device was used for the *UV-Vis spectral analysis* of nanoparticles formed under different conditions. To determine the formation of Ag and Zn nanoparticle synthesis, laurel extract reacted with $AgNO_3$ and $Zn(Ac)_2 \cdot H_2O$, and the samples were analysed using *FTIR spectroscopy* with a Shimadzu IR Affinity-1 instrument. Morphological properties were studied by *scanning electron microscopy* using a TESCAN MAIA3 XMU instrument. Finally, *XRD analysis* was performed to determine the nanoparticle crystal structure using a Rigaku Smartlab instrument with a step pitch of 0.02° 2θ and an increment rate of 2° 2θ/min.

Extraction of laurel leaves

LB-AgNPs and LB-ZnNPs were synthesized using laurel extract as a reducing agent. Laurel leaves (*Laurus nobilis*) were collected in Balamba, Bartin province. After thorough washing with tap and distilled water, the leaves were dried. For nanoparticle synthesis, dried laurel leaves were boiled in distilled water for 1 h. The resulting extract was filtered to remove impurities and stored at +4°C for future use.

Biosynthesis of Ag and Zn nanoparticles

Well washed bay leaves were mixed with deionized water in a blender and a homogeneous extract was obtained. The extract was filtered through a glass strainer and cleaned. An amount of 0.01 mol 20 mL $AgNO_3$ and $Zn(Ac)_2 \cdot 2H_2O$ salts were dissolved separately in deionized water. A certain amount of 50 mL of the prepared bay leaf extract was added to the $AgNO_3$ and $Zn(Ac)_2 \cdot 2H_2O$ solutions separately, and a homogeneous mixture was obtained. The reaction temperature was controlled by heating at 70°C using a water bath. The reaction progress was monitored by UV-Vis spectroscopy. The spectroscopy was scanned in the range of 200-800 nm, and plasmonic resonance peaks were observed. The effects of reaction time and $AgNO_3$/laurel extract and $Zn(Ac)_2 \cdot H_2O$/laurel extract ratios on the formation of Ag and Zn nanoparticles were investigated. The obtained nanoparticles were washed twice with distilled water and twice with alcohol, dried in a vacuum oven, and swollen for characterization analysis. As a result of the experiment, LB-AgNPs and LB-ZnNPs were synthesized.

Determination of the photocatalytic properties

The photocatalytic properties of the obtained nanoparticles were evaluated by UV-Vis spectroscopy. For this purpose, the model

compound, methylene blue (10^{-5} M), was placed in a quartz cuvette (3×10^{-3} L), and varying amounts of catalyst were added. The photocatalytic activity of LB-AgNPs and LB-ZnNPs was investigated by degrading methylene blue dye in quartz tubes under UV light irradiation. An unfiltered UV-C tube lamp (15 W, length 41 cm, diameter 2.5 cm), model G15T8 (Philips, Holland), was utilized as the irradiation source (λ= 254 nm). Changes in the absorption were observed every 30 min using a UV-Visible absorption spectroscopy. The same procedure was repeated to determine the activity of the photocatalyst in the dark. After determining the catalyst amount (1.6 mg/3×10^{-3} L), the effect of this catalyst amount on the dye was examined.

Results and discussion
UV-Vis and FTIR analysis results

Yassin, M.T. *et al.* stated that the main peak observed in the UV spectrum of AgNPs between 242 and 300 nm is associated with biomolecules in the plant extract [21]. They also stated that the peak at 374 nm was assigned to biogenic AgNPs. The results obtained demonstrate the successful formation of AgNPs by the transition from 374 nm to 444 nm because of the intervention of biomolecules in the plant extract [22,23]. In a previously performed study [24], the main feature of ZnO NPs produced with thyme leaf extract is that they have a high absorbance in the UV region below 400 nm and a low absorbance in the visible region. The results of the UV-Vis spectroscopy analysis showed excellent agreement with those of previous studies [24].

The formation of silver and zinc nanoparticles was confirmed through UV-Vis analysis (Figure 1). The reduction of Ag^+ ions to Ag^0 metals in the LB-AgNP complex using laurel leaf extract resulted in the excitation of surface plasmon resonance, which was measured using UV-Vis spectroscopy. The UV-Vis spectral peaks of LB-AgNPs were recorded at 375 and 383 nm. The UV-Vis spectral peaks of LB-ZnNPs were recorded at 350 and 354 nm, respectively.

The UV-Vis analysis results demonstrate that Ag and Zn nanoparticles have been successfully synthesized. To support this result and determine the pathways of Ag and Zn nanoparticle synthesis, FTIR spectra of the obtained nanoparticles were obtained. The presence of various functional groups in the molecules responsible for the biological reduction and stabilization of LB-AgNPs was determined by FTIR analysis. The observed intense bands were compared with standard values to identify the

functional groups. The value of 1243.86 cm^{-1} was obtained from the CN stretching, and the bending of NH, which is the most probable composition for amid-III to be an oxime, was obtained at 3597.54 cm^{-1} (Figure 2) [25]. Since the plant extract used in both nanoparticles is the same, similar peaks are seen at similar points. For example, the peak seen in both nanoparticles in the 3200-3500 cm^{-1} range is due to the O-H stretching of alcohol and phenolic compounds. These compounds are often shown to be directly responsible for the reduction in Ag and Zn. The band around 3000 cm^{-1} is due to the aromatic C-H stretching mode. The absorption peak at 1550 cm^{-1} is due to C-C in the aromatic ring. The peak at 1380 cm^{-1} is due to the C-O-C stretching mode. These peaks are similar to those reported in previous studies.
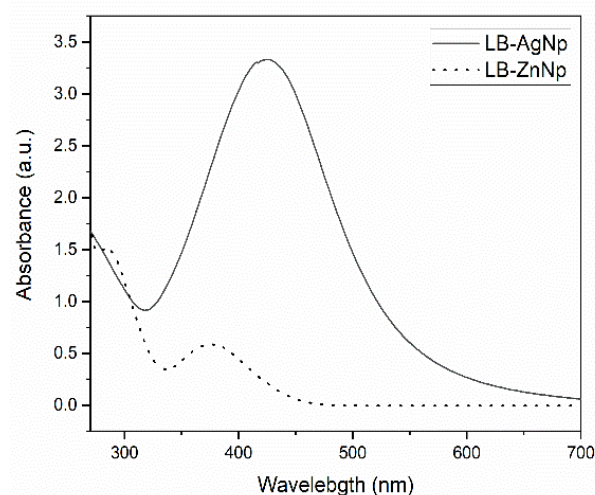

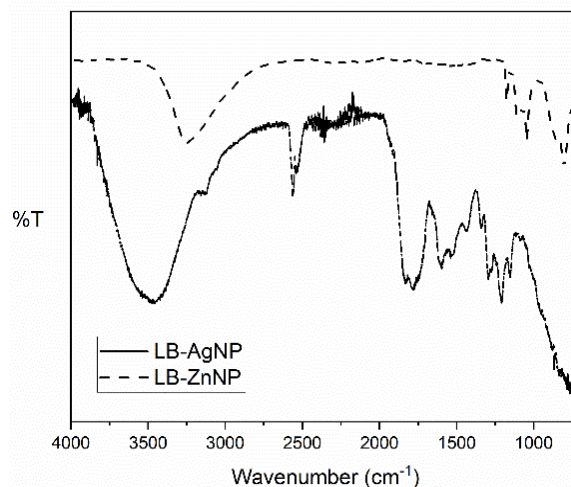**Figure 1. The UV-Vis spectra of biosynthesized LB-AgNPs and LB-ZnNPs.**

Figure 2. The FTIR spectra of LB-AgNP LB-ZnNPs were obtained using the biosynthesis method.

XRD analysis results

The XRD patterns of the LB-AgNPs and LB-ZnNPs are shown in Figure 3. On the basis of the XRD analysis results of LB-AgNPs, the obtained data provide information about the crystal structure and dimensions. The most prominent peak in the graph is observed at approximately 38 degrees in the 2θ angle. This peak may reflect a fundamental characteristic of the crystalline structure of silver nanoparticles. This peak at a 2θ angle is quite close to the typical value of 38.2 degrees for silver in the JCPDS card no. 04-0783 database, indicating that the crystal structure of silver nanoparticles consists of silver atoms. The most prominent peak in the XRD pattern of LB-ZnNPs is observed at approximately 36 degrees in the 2θ angle. This peak may reflect a fundamental characteristic of the crystalline structure of zinc nanoparticles. This peak at a 2θ angle is quite close to the typical value of 36.4 degrees for zinc in the JCPDS card no. 79-2205 database, indicating that the crystal structure of zinc nanoparticles consists of zinc atoms.

The widths of the peaks in the XRD pattern are associated with the nanoparticle size and interplanar spacing. The broad and low-intensity background of the peaks may indicate a wide size distribution of nanoparticles and the presence of nanoparticles of different sizes. This wide size distribution suggests that the silver and zinc nanoparticles obtained through biosynthesis may have a heterogeneous structure. In addition, other peaks or small clusters of peaks in the XRD pattern may reflect different surface arrangements or defects in the crystal structure of nanoparticles.

These defects may arise from variations in the biosynthesis process of nanoparticles and can affect interplanar bonding.

In the study by Gul, R. *et al.*, measurements were made between 2θ 20 and 80° for Ag nanoparticles obtained from *Kalanchoe tubiflora* [26]. The results show that four Bragg peaks corresponding to the 111, 200, 220, and 311 crystal planes of Kt-AgNPs are well observed and are located at 38.22°, 46.32°, 64.34°, and 76.46°, respectively [26]. Karam, S.T. *et al.* obtained ZnO NPs from thyme leaves and found that the average particle sizes measured along the diffraction peak (002) of biosynthesized ZnO NPs were 35.202, 35.203, 56.249, and 63.308 [24].

SEM results

On the basis of the SEM analysis results of zinc nanoparticles, information about nanoparticle morphology and distribution can be obtained. The observed images reveal the surface characteristics of the zinc nanoparticles obtained through biosynthesis. In the SEM images of LB-AgNPs, round or oval-shaped nanoparticles are generally observed. These round or oval shapes could be indicative of the silver crystal structure of the nanoparticles and may be associated with the biosynthesis process (Figure 4*(a)*). Furthermore, upon examining the SEM images of LB-ZnNPs, it was determined that the nanoparticle structures were rod-like in shape (Figure 4*(b)*). The size distribution of the nanoparticles can also be estimated from the SEM images. The nanoparticles of various sizes can be observed in the images. These nanoparticles of different sizes may arise from variations in the biosynthesis process, nucleation, and growth mechanisms.
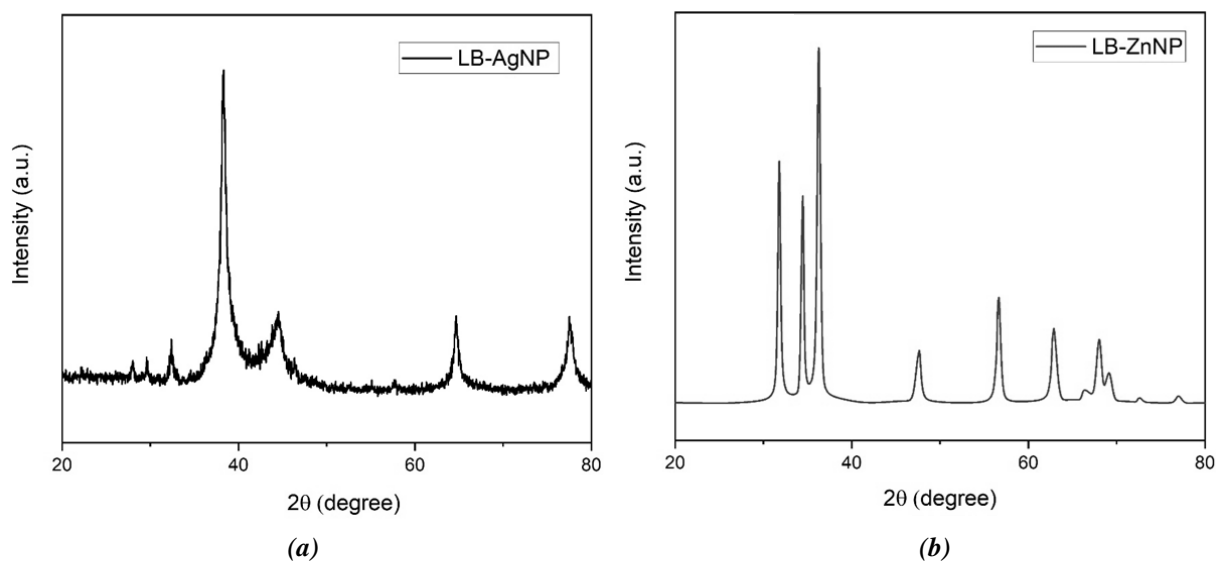

(a)   *(b)*

Figure 3. XRD spectra of the biosynthesized LB-AgNP *(a)* and biosynthesized LB-ZnNPs *(b).*

In addition, in the SEM images, it may be observed that nanoparticles tend to agglomerate or bind to each other. These agglomerations could be a result of the surface energies or interactions of the nanoparticles. The presence of agglomerations indicates that silver and zinc nanoparticles can combine to form aggregates with different structural properties. In addition, irregularities or surface defects of nanoparticles may be observed in the SEM images. These irregularities could be a reflection of the structural changes that occur during the biosynthesis process. In conclusion, SEM analysis revealed the surface morphology, size distribution, and agglomeration tendency of silver and zinc nanoparticles obtained through biosynthesis.

Photocatalysis results

First, a catalyst amount study was conducted to determine the amount of catalyst to be used.

For this purpose, the model compound, methylene blue (10^{-5} M), was placed in a quartz cuvette (3×10^{-3} L), and varying amounts of catalyst were added. Changes in the absorption were observed every 30 min using a UV-Visible absorption spectroscopy. The same procedure was repeated to determine the activity of the photocatalyst in the dark. After determining the catalyst amount (1.6 mg/3×10^{-3} L), the effect of this catalyst amount on the dye was examined.

The photocatalytic degradation of methylene blue was investigated in the presence of LB-AgNPs under a UV light source. The changes in the absorption spectra of methylene blue in the presence of LB-AgNPs under UV light are shown in Figure 6. The intensity of the absorption bands of the dyes decreased in the presence of the catalyst.
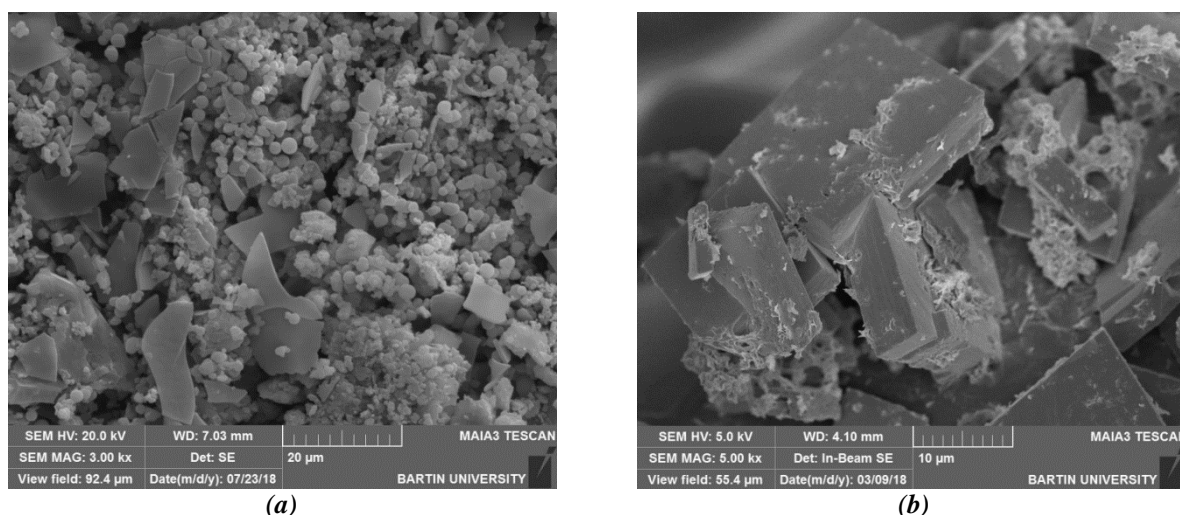

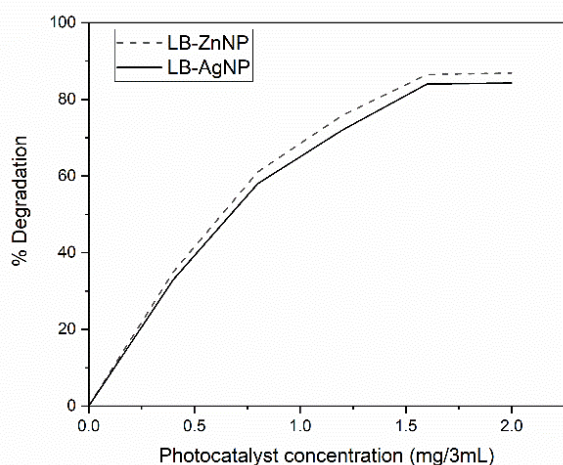**Figure 4. SEM images of the obtained nanoparticles, LB-AgNP *(a)* and LB-ZnNP *(b)*.**

Figure 5. The percentages of methylene blue degradation with different quantities of nanoparticles which were used as catalysts.
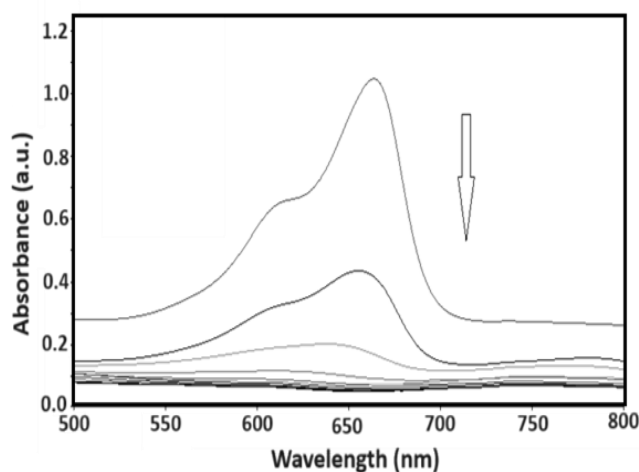
Figure 6. Changes of the UV-Vis spectrum of the methylene blue as a function of time in the presence of the LB-AgNP catalyst.

As shown in Figure 7, the characteristic absorption band of methylene blue at 640 and 664 nm has disappeared in the presence of the LB-AgNP catalyst after 150 min. At the end of 150 min, methylene blue was degraded by 97.5% in the presence of the LB-AgNP catalyst. Figure 8 illustrates the changes in the degradation efficiency of methylene blue organic dye in the presence of the catalyst and light sources as a function of irradiation time. Three different experiments were conducted to investigate the effect of the light source on the catalyst/dye system. In the first experimental set, the photolysis effect of the dye in the presence of the catalyst under UV light was examined. In the second experimental set, the degradation of the dye under UV light without the catalyst was studied. The results indicated that the dye did not exhibit a photolysis effect in the absence of the catalyst. In the third experimental set, the effect of the light source was investigated by adding the catalyst to the organic dye and

keeping it in the dark. When the data obtained from these three experimental sets were compared, it was observed that the catalysts were much more effective under UV light than in a dark environment.

A reusability study was conducted using the determined catalyst amount and a concentration of 10^{-5} M for the photocatalyst. For this purpose, after the photocatalyst completely degraded the dye, it was separated from the dye, thoroughly washed with distilled water, dried, and used for subsequent cycles. The same process was repeated for 4 catalyst reuses. According to these results, the LB-AgNP photocatalyst degraded the dye by 97.5% in its first use. Although it decreased up to 80% in reuse, it is seen that it is possible to use LB-AgNP material as a photocatalyst when compared with the literature [27]. Furthermore, it was clearly demonstrated that the LB-AgNP catalyst has higher stability than the LB-ZnNP catalyst and thus can be used in many cycles and for a long time.
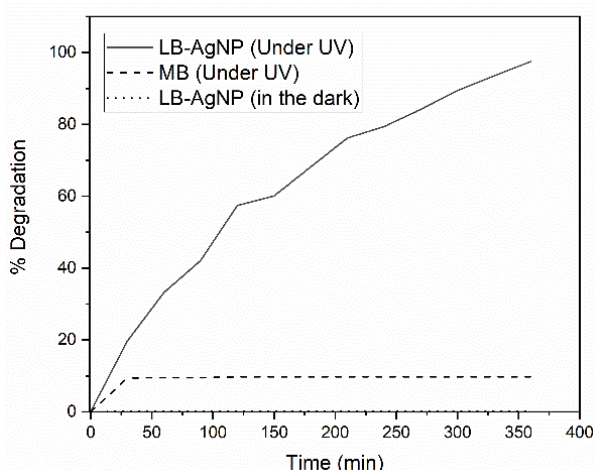

Figure 7. Comparison of the degradation of the model compound dye in the presence of LB-AgNP catalyst under UV light, in the dark, and without catalyst under UV light.
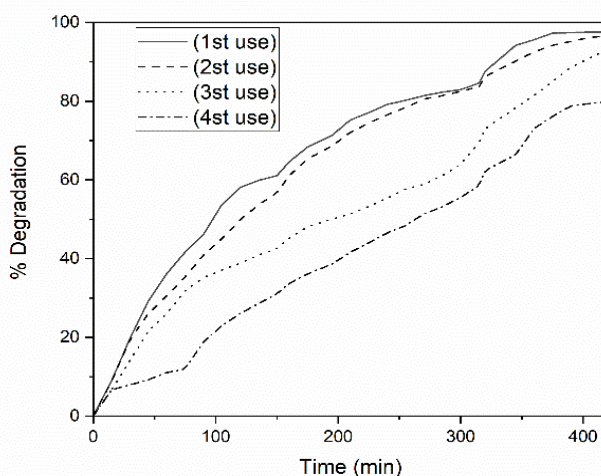

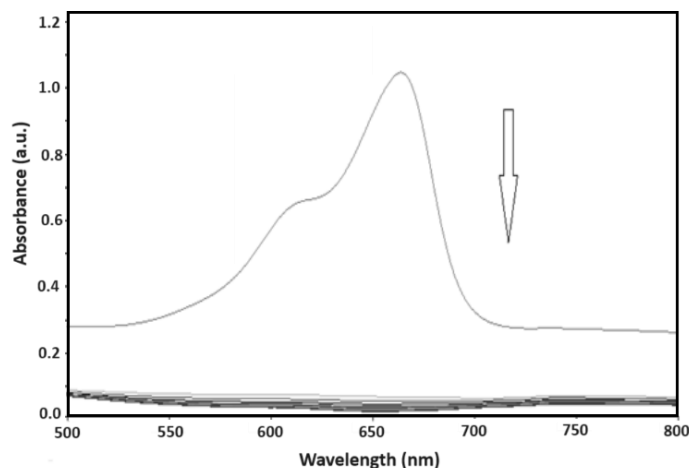**Figure 8. The reusability of the LB-AgNP material as photocatalyst.**

Figure 9. UV spectrum of methylene blue pollutant as a function of time in the presence of the LB-ZnNP catalyst.

The photocatalytic degradation of methylene blue was investigated in the presence of LB-ZnNPs under a UV light source. The changes in the absorption spectra of methylene blue in the presence of LB-ZnNPs under UV light are shown in Figure 9. The intensity of the absorption bands of the dyes decreased in the presence of the catalyst, but to a lesser extent compared with LB-AgNPs. As shown in the Figure 9, the characteristic absorption band of methylene blue at 640 and 664 nm rapidly disappeared in the presence of the LB-ZnNP catalyst.

In Figure 10, the changes in the degradation efficiency of the organic dye, methylene blue, under different light sources in the presence of the catalyst are shown as a function of irradiation time. Three different experiments were conducted to investigate the effect of the light source on the catalyst/dye system. In the first experimental set, the photolysis effect of the dye in the presence of the catalyst under UV light was examined. In the second experimental set, the degradation of the dye under UV light without the catalyst was studied.
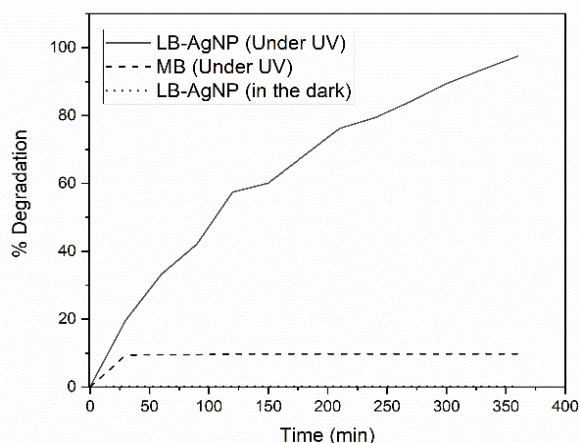

Figure 10. Comparison of the degradation of the model compound dye in the presence of LB-ZnNP catalyst under UV light, in the dark, and without catalyst under UV light.
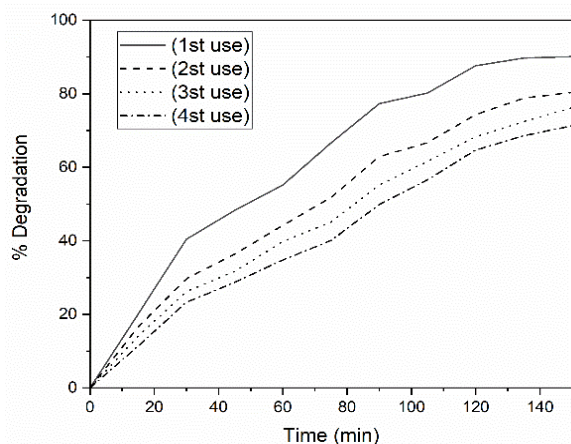

Figure 11. The reusability of LB-ZnNP catalyst.

The results indicated that the dye did not exhibit a photolysis effect in the absence of the catalyst. In the third experimental set, the effect of the light source was investigated by adding the catalyst to the organic dye and keeping it in the dark. When the data obtained from these three experimental sets were compared, it was observed that the catalysts were much more effective under UV light than in a dark environment.

A reusability study was conducted with the determined amount of catalyst and 10^{-5} M concentration for the photocatalyst (Figure 11). For this purpose, after the photocatalyst completely degraded the dye, it was separated from the dye, thoroughly washed with distilled water, dried, and used for subsequent cycles. The same process was repeated for four catalyst reuses. The results obtained showed that the LB-ZnNP photocatalyst degraded the dye by 90.9% in the first use, whereas this rate decreased to approximately 70% in the fourth use. This shows that the use of this material as a photocatalyst is promising.

Conclusions

In this study, silver and zinc nanoparticles were synthesized and characterized through green synthesis using bay leaf extract. The characterization of these nanoparticles involved UV-Vis spectroscopy FTIR spectroscopy, SEM imaging, and XRD analysis. The UV-Vis spectroscopy results indicated the presence of a prominent band at 444 nm, confirming the formation of silver nanoparticles, and another band at 374 nm, confirming the formation of zinc nanoparticles. In addition, functional groups from the bay leaf extract were identified in the FTIR spectrum. The crystal structures of the biosynthesized LB-AgNPs and LB-ZnNPs were analyzed through XRD. SEM images revealed the morphologies of the nanoparticles, with LB-AgNPs generally exhibiting round and oval shapes, while LB-ZnNPs displayed rod-like structures. Furthermore, the photocatalytic properties of the nanoparticles were investigated, and it was found that LB-AgNPs achieved a degradation percentage of 97.5%, whereas LB-ZnNPs achieved a degradation percentage of 90.9%. LB-ZnNPs demonstrated superior photocatalytic performance.

This study highlights the influence of bay leaf extract in biosynthesis on the photocatalytic properties of silver and zinc nanoparticles. Optimizing the synthesis conditions and bay leaf extract concentrations may further enhance their photocatalytic activity. Moreover, the addition of various additives or surface modification

techniques could be explored to improve photocatalytic efficiency. On the basis of these findings, LB-AgNPs and LB-ZnNPs hold promise as photocatalysts for water pollutant removal and the degradation of toxic organic compounds.

Acknowledgements

References

1. Sinha, S.N.; Paul, D.; Halder, N.; Sengupta, D.; Patra, S.K. Green synthesis of silver nanoparticles using fresh water green alga *Pithophora oedogonia* (Mont.) Wittrock and evaluation of their antibacterial activity. Applied Nanoscience, 2005, 5, pp. 703−709. DOI: https://doi.org/10.1007/s13204-014-0366-6

2. Vithiya, K.; Sen, S. Biosynthesis of Nanoparticles. International Journal of Pharmaceutical Sciences and Research, 2011, 2(11), pp. 2781−2785. DOI: http://doi.org/10.13040/IJPSR.0975-8232.2(11).2781-85

3. Mohanpuria, P.; Rana, N.K.; Yadav, S.K. Biosynthesis of nanoparticles: technological concepts and future applications. Journal of Nanoparticle Research, 2008, 10, pp. 507−517. DOI: https://doi.org/10.1007/s11051-007-9275-x

4. Manojkumar, U.; Kaliannan, D.; Srinivasan, V.; Balasubramanian, B; Kamyab, H.; Mussa, Z.H.; Palaniyappan, J.; Mesbah, M.; Chelliapan, S.; Palaninaicker, S. Green synthesis of zinc oxide nanoparticles using *Brassica oleracea* var. botrytis leaf extract: Photocatalytic, antimicrobial and larvicidal activity. Chemosphere, 2023, 323, pp. 138263. DOI: https://doi.org/10.1016/j.chemosphere.2023.138263

5. Basuliman, M.M.; Bamahel, A.S.; Al-Kathiri, D.G.; Al-Suhily, A.M. The effect of various concentrations of $AgNO_3$ aqueous solutions on silver nanoparticles biosynthesis using *Tarchonanthus camphoratus* leaf extract and their antibacterial activity. Moroccan Journal of Chemistry, 2023, 11(2), pp. 361−370. DOI: https://doi.org/10.48317/IMIST.PRSM/morjchem-v11i1.33269

6. Yaqoob, A.A.; Umar, K.; Ibrahim, M.N.M. Silver nanoparticles: various methods of synthesis, size affecting factors and their potential applications–a review. Applied Nanoscience, 2020, 10, pp. 1369−1378. DOI: https://doi.org/10.1007/s13204-020-01318-w

7. Dat, N.M.; Linh, V.N.P.; Huy, L.; Huong, N.T.; Tu, T.H.; Phuong, N.T.L.; Nam, H.M.; Phong, M.T.; Hieu, N.H. Fabrication and antibacterial activity against Pseudomonas aeruginosa and Staphylococcus aureus of silver nanoparticle decorated reduced graphene oxide nanocomposites. Materials Technology, 2019, 34(7), pp. 369−375. DOI: https://doi.org/10.1080/10667857.2019.1575555

8. Ponnamma, D.; Cabibihan, J.J.; Rajan, M.; Pethaiah, S.S.; Deshmukh, K.; Gogoi, J.P.; Pasha, S.K.K.; Ahamed, M.B.; Krishnegowda, J.; Chandrashekar, B.N.; Polu, A.R.; Cheng, C. Synthesis, optimization and applications of ZnO/polymer nanocomposites. Materials Science and Engineering: C, 2019, 98, pp. 1210−1240. DOI: https://doi.org/10.1016/j.msec.2019.01.081

9. Rajendrachari, S.; Kamaci, Y.; Tas, R.; Ceylan, Y.; Bulbul, A.S.; Uzun, O.; Karaoglanli, A.C. Antimicrobial investigation of CuO and ZnO nanoparticles prepared by a rapid combustion method. Physical Chemistry Research, 2019, 7(4), pp. 799−812. DOI: https://doi.org/10.22036/PCR.2019.199338.1669

10. Ma, L.; Liu, B.; Huang, P.J.; Zhang, X.; Liu, J. DNA adsorption by ZnO nanoparticles near its solubility limit: implications for DNA fluorescence quenching and DNAzyme activity assays. Langmuir, 2016, 32(22), pp. 5672−5680. DOI: https://doi.org/10.1021/acs.langmuir.6b00906

11. Chupani, L.; Zuskova, E.; Niksirat, H.; Panacek, A.; Lunsmann, V.; Haange, S.B.; von Bergen, M.; Jehmlich, N. Effects of chronic dietary exposure of zinc oxide nanoparticles on the serum protein profile of juvenile common carp (*Cyprinus carpio* L.). Science of the Total Environment, 2017, 579, pp. 1504−1511. DOI: https://doi.org/10.1016/j.scitotenv.2016.11.154

12. Taban, A.; Saharkhiz, M.J.; Niakousari, M. Sweet Bay (*Laurus nobilis* L.) essential oil and its chemical composition, antioxidant activity and leaf micromorphology under different extraction methods. Sustainable Chemistry and Pharmacy, 2018, 9, pp. 12−18. DOI: https://doi.org/10.1016/j.scp.2018.05.001

13. Curco, D.; Gimenez, J.; Addardak, A.; Cervera-March, S.; Esplugas, S. Effects of radiation absorption and catalyst concentration on the photocatalytic degradation of pollutants. Catalysis Today, 2002, 76(2-4), pp. 177−188. DOI: https://doi.org/10.1016/S0920-5861(02)00217-1

14. Ravishankar, T.N.; Manjunatha, K.; Ramakrishnappa, T.; Nagaraju, G.; Kumar, D.; Sarakar, S.; Anandakumar, B.S.; Chandrappa, G.T.; Reddy, V.; Dupont, J. Comparison of the photocatalytic degradation of trypan blue by undoped and silver-doped zinc oxide nanoparticles. Materials Science in Semiconductor Processing, 2014, 26, pp. 7−17. DOI: https://doi.org/10.1016/j.mssp.2014.03.027

15. Rajendran, R.; Mani, A. Photocatalytic, antibacterial and anticancer activity of silver-doped zinc oxide nanoparticles. Journal of Saudi Chemical Society, 2020, 24(12), pp. 1010−1024. DOI: https://doi.org/10.1016/j.jscs.2020.10.008

16. Marimuthu, S.; Antonisamy, A.J.; Malayandi, S.; Rajendran, K.; Tsai, P.C.; Pugazhendhi, A.; Ponnusamy, V.K. Silver nanoparticles in dye effluent treatment: A review on synthesis, treatment methods, mechanisms, photocatalytic degradation, toxic effects and mitigation of toxicity. Journal of Photochemistry and Photobiology B: Biology, 2020, 205, pp. 111823. DOI: https://doi.org/10.1016/j.jphotobiol.2020.111823

17. Danish, M.S.S.; Estrella-Pajulas, L.L.; Alemaida, I.M.; Grilli, M.L.; Mikhaylov, A.; Senjyu, T. Green synthesis of silver oxide nanoparticles for photocatalytic environmental remediation and

biomedical applications. Metals, 2022, 12(5), pp. 769−789.
DOI: https://doi.org/10.3390/met12050769

18. Dihom, H.R.; Al-Shaibani, M.M.; Mohamed, R.M.S.R.; Al-Gheethi, A.A.; Sharma, A.; Khamidun, M.H.B. Photocatalytic degradation of disperse azo dyes in textile wastewater using green zinc oxide nanoparticles synthesized in plant extract: A critical review. Journal of Water Process Engineering, 2022, 47, pp. 102705.
DOI: https://doi.org/10.1016/j.jwpe.2022.102705

19. Kumar, R.V.; Vinoth, S.; Baskar, V.; Arun, M.; Gurusaravanan, P. Synthesis of zinc oxide nanoparticles mediated by *Dictyota dichotoma* endophytic fungi and its photocatalytic degradation of fast green dye and antibacterial applications. South African Journal of Botany, 2022, 151(B), pp. 337−344.
DOI: https://doi.org/10.1016/j.sajb.2022.03.016

20. Al Hazmi, R.; Oudghiri-Hassani, H.; Al Wadaani, F.; Abboudi, M. High performance photocatalytic activity of Mg^{2+} doped hexagonal ZnO nanoparticles in the methylene blue degradation under UV irradiation. Moroccan Journal of Chemistry, 2016, 4(2), pp. 324−331. DOI: https://doi.org/10.48317/IMIST.PRSM/morjchem-v4i2.4270

21. Yassin, M.T.; Mostafa, A.A.F.; Al-Askar, A.A.; Al-Otibi, F.O. Facile green synthesis of silver nanoparticles using aqueous leaf extract of *Origanum majorana* with potential bioactivity against multidrug resistant bacterial strains. Crystals, 2022, 12(5), pp. 603−610.
DOI: https://doi.org/10.3390/cryst12050603

22. Delgado-Beleño, Y.; Martínez-Núñez, C.E.; Flores-López, N.S.; Meza-Villezcas, A.; Ramírez-Rodríguez, L.P.; Britto Hurtado, R.; Flore-Acosta, M.; Cortez-Valadez, M. Characterization of silver nanoparticles encapsulated using an ion-exchange-mediated method and their application as antimicrobial agents. Journal of Electronic Materials, 2021, 50, pp. 5632-5638.
DOI: https://doi.org/10.1007/s11664-021-09089-y

23. Heinemann, M.G.; Rosa, C.H.; Rosa, G.R.; Dias, D. Biogenic synthesis of gold and silver nanoparticles used in environmental applications: A review. Trends in Environmental Analytical Chemistry, 2021, 30, pp. e00129.
DOI: https://doi.org/10.1016/j.teac.2021.e00129

24. Karam, S.T.; Abdulrahman, A.F. Green synthesis and characterization of ZnO nanoparticles by using thyme plant leaf extract. Photonics, 2022, 9(8), pp. 594−614.
DOI: https://doi.org/10.3390/photonics9080594

25. Rasool, S.; Raza, M.A.; Manzoor, F.; Kanwal, Z.; Riaz, S.; Iqbal, M.J.; Naseem, S. Biosynthesis, characterization and anti-dengue vector activity of silver nanoparticles prepared from *Azadirachta indica* and *Citrullus colocynthis*. Royal Society Open Science, 2020, 7(9), pp. 200540.
DOI: https://doi.org/10.1098/rsos.200540

26. Gul, R.; Naqib, S.; Saleh, E.A.M.; Khan, S.U.; Ibrahim, M.; Tabassum, S.; Zaman, U.; Rehman, K.; Khan, D.; Rizg, W.Y.; Hosny, K.M.; Alissa, M.; Bukhary, S.M.; Alkhalidi, H.M. An eco-benign biomimetic approach for the synthesis of novel silver nanoparticles (Kt-AgNPs): Ultra efficient nanoparticles with enhanced biomedical applications. Inorganic Chemistry Communications, 2023, 155, pp. 111109.
DOI: https://doi.org/10.1016/j.inoche.2023.111109

27. Al-Gharibi, M.A.; Kyaw, H.H.; Al-Sabahi, J.N.; Myint, M.T.Z.; Al-Sharji, Z.A.; Al-Abri, M.Z. Silver nanoparticles decorated zinc oxide nanorods supported catalyst for photocatalytic degradation of paracetamol. Materials Science in Semiconductor Processing, 2021, 134, pp. 105994.
DOI: https://doi.org/10.1016/j.mssp.2021.105994